Quantitative Measurement of Transmission, Reflection, and Diffraction of Two-Dimensional Photonic Band Gap Structures at Near-Infrared Wavelengths

D. Labilloy,[1] H. Benisty,[1] C. Weisbuch,[1] T. F. Krauss,[2,*] R. M. De La Rue,[2] V. Bardinal,[3,†] R. Houdré,[3] U. Oesterle,[3] D. Cassagne,[4] and C. Jouanin[4]

[1]*Laboratoire de Physique de la Matière Condensée, Ecole Polytechnique, URA 1254 CNRS, 91128 Palaiseau Cedex, France*
[2]*Department of Electronics and Electrical Engineering, Glasgow University, G12 8LT, Glasgow, United Kingdom*
[3]*Institut de Micro et Opto-électronique, Ecole Polytechnique Fédérale de Lausanne, CH-1015 Lausanne, Switzerland*
[4]*Groupe d'Etudes des Semiconducteurs, Université Montpellier II CC074, place E. Bataillon, 34095 Montpellier Cedex 05, France*

(Received 22 July 1997)

We present quantitative measurements of the interaction between a guided optical wave and a two-dimensional photonic crystal using spontaneous emission of the material as an internal point source. This is the first analysis at near-infrared wavelengths where transmission, reflection, and in-plane diffraction are quantified at the same time. Low transmission coincides with high reflection or in-plane diffraction, indicating that the light remains guided upon interaction. Also, good qualitative agreement is found with a two-dimensional simulation based on the transfer matrix method. [S0031-9007(97)04591-2]

PACS numbers: 42.70.Qs, 42.25.–p, 42.50.–p, 42.82.–m

Photonic band gap (PBG) structures are of great interest for both fundamental and application-driven reasons [1–3]. They are periodic dielectric structures that are designed to affect electromagnetic wave propagation in the same way as the periodic electrostatic potential in a crystal structure affects the electron motion by defining allowed and forbidden (the gap) electronic energy bands. They open the possibility of manipulating electromagnetic wave emission and propagation processes. As a result, novel types of light sources with high electrical to optical conversion efficiency, directionality, spectral narrowing, and sub-Poissonian noise can be expected [1,4].

A first step towards achieving these goals is the demonstration of the basic properties of photonic crystals such as good transmission or reflection coefficients in the allowed or forbidden energy regions, respectively, and minimal losses. So far, experimental determination of gaps in the near-infrared or visible range relies on partial data, e.g., only transmission, in both the two- (2D) and three-dimensional (3D) cases [5–8].

Although not as general as 3D structures, 2D photonic crystals, e.g., when etched through a waveguide, are still in very high demand as they provide a convenient way of controlling in-plane spontaneous emission in heterostructures, a major source of loss in vertical-emitting structures [9,10]. However, some observations of scattering of light out of the PBG plane [11–13] have given rise to the concern that the finite height of the holes and the waveguide geometry might lead to strong scattering of light into the substrate or the free space above the sample, which may preclude the use of PBG structures in integrated optics. Complementary transmission and reflection data is, therefore, all the more urgently needed to clarify this issue.

Our experiments use photoluminescence (PL) as an in-built point source in a planar waveguide configuration [Fig. 1(a)]. The guided emission impinges on a slab of 2D PBG structure that has been deeply etched through the waveguide. By comparison with an unprocessed area, the reflection, transmission, and diffraction coefficients of the photonic crystal can be determined. This set of measurements fully describes the interaction of the guided mode with the photonic crystal and, in particular, the transformation of transmitted into reflected light at a band edge.

A movable internal point source is obtained from the focused spot of a red laser diode (678 nm) which excites the photoluminescence of three $In_{0.17}Ga_{0.83}As$ strained quantum wells (QWs) embedded in a 250 nm wide GaAs single-mode waveguide with $Al_{0.80}Ga_{0.20}As$ barriers, 400 and 30 nm wide, respectively. In our particular design, the guide captures about 40% of the emitted PL [14].

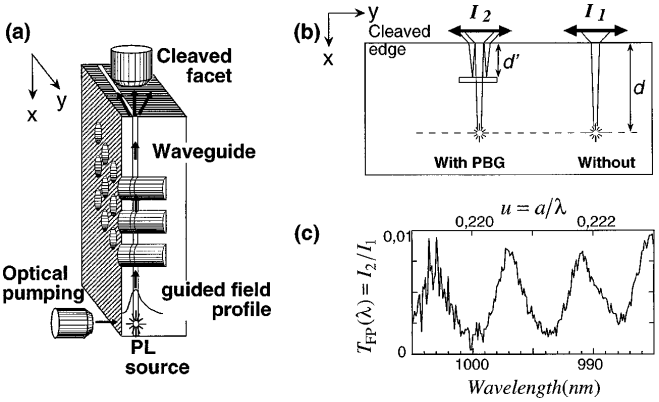

FIG. 1. (a) Schematic of experiment. (b) Side view of (a): configuration for measurements at normal incidence. The rectangle features the PBG slab. Multiple-beam interferences occur between the cleaved edge and the PBG pattern. (c) Typical experimental transmission spectrum in an $a = 220$ nm sample.

The in-plane radiation pattern is isotropic, and consists of circular waves. This light probes the photonic structure before leaving the sample by a cleaved facet, where it is collected with a microscope equipped with polarizers. The beam is then split between a CCD camera for observation and a multimode fiber, which collects a known disk of light in the magnified image of the sample edge for spectral analysis. This system features a 4 μm spatial resolution for the spectral analysis with a $\times 20$ objective (numerical aperture $= 0.4$). As detailed elsewhere [15], the guided part of the PL emission is easily separated from the radiation into substrate and air, when the distance d from the source to the cleaved edge is larger than 30 μm. Furthermore, only rays with a maximum internal angle of $\pm 6°$ with respect to the normal of the cleaved edge are collected by the objective, due to its limited numerical aperture and the high index of refraction ($n_{\text{eff}} \approx 3.4$) of the waveguide. Using this natural angular selectivity, the PBG pattern is essentially probed by those rays normal to the cleaved edge, i.e., it is probed along the x axis of Figs. 1(a) and 1(b).

Here, PBG patterns are defined by e-beam lithography followed by deep reactive ion etching [6,16]. They consist of a triangular array of cylindrical holes with a lattice parameter a varying from 180 to 360 nm. We chose a moderate filling factor f (ratio of holes to total area) of between 25 and 30% to minimize radiation losses into the air and the substrate [6]. In this (a, f) range, the hole depth (about 0.8 μm) is reasonably constant, with straight side walls [6], so that the patterns interact with more than 95% of the guided mode. Two types of patterns were fabricated, with either the ΓM or the ΓK principal crystallographic axis of the Brillouin zone, aligned along the x axis [17].

In this Letter, we shall focus mostly on transmission and reflection at normal incidence and will discuss in-plane diffraction on a selected example. For these measurements, we take the ratio of intensities I_2/I_1 collected when guided light traverses a deep-etched PBG pattern of period a and a nearby unprocessed area [Fig. 1(b)]. The ratio of these two measurements eliminates all other interface and absorption effects in the guide and thus gives the PBG effect alone [15]. Because of the strain in the QWs, the guided emission is polarized: mostly TE (**E** in the guide plane) for heavy hole transitions (980 nm), mostly TM (**H** in the guide plane) for light hole transitions (930 nm). The useful spectral range in the particular heterostructure used in this experiment is approximately 20 nm, centered at 995 and 940 nm for TE and TM polarizations, respectively, and is limited by reabsorption of guided light in the waveguide.

We can extract transmission and reflection data from a single measurement. The material section between the parallel cleaved edge and the PBG pattern forms a slab of thickness d' bounded with partially reflecting boundaries: the cleaved facet and the pattern [Fig. 1(b)]. Therefore, guided waves undergo in-plane multiple-beam interferences. In the plane-wave approximation, the ratio I_2/I_1 then amounts to the well-known Fabry-Perot transmission

$$T_{\text{FP}}(\lambda) = \left| \frac{t}{1 - rr_2 \exp(2i\Phi) \exp(-\alpha d')} \right|^2,$$

where t is the amplitude transmission, r is the amplitude reflection coefficient of the photonic crystal, and r_2 is the amplitude reflection coefficient of the cleaved edge; $2\Phi = 4\pi d' n_{\text{eff}}/\lambda$ is the round-trip phase and $\exp(-\alpha d')$ is the absorption, both at normal incidence. If $\alpha d' \gg 1$, spectral oscillations appear in the ratio $T_{\text{FP}}(\lambda)$ [see Fig. 1(c)]. We separately extract α from $I_1(d) \propto \exp(-\alpha d)/d$ by varying d; r_2 is the known Fresnel reflection coefficient for the cleaved edge at normal incidence ($r_2 \approx 55\%$). It is then straightforward to deduce $T(\lambda) = |t|^2$ and $R(\lambda) = |r|^2$ on the small corresponding range of $u = a/\lambda$ from the mean value and the fringe visibility $V = (T_{\text{FP}}^{\max} - T_{\text{FP}}^{\min})/(T_{\text{FP}}^{\max} + T_{\text{FP}}^{\min})$ [18]. We performed these measurements on seven different samples with periods a varying from 180 to 360 nm ($u = 0.18$ to 0.38) in order to obtain data on a larger range of u. For each sample, we extract the following data from $T_{\text{FP}}(\lambda)$ across the 20-nm-wide useful range: the transmission value $T(u)$ at 995 and 940 nm for TE and TM polarization, respectively, the derivative $\partial T(u)/\partial u$, and the fringe visibility V, in order to calculate the reflection coefficient R. In the example of Fig. 1(c), $T(u) \approx 5 \times 10^{-3}$ at 995 nm, the derivative is slightly positive and the fringe visibility is 67%. Given $\alpha d' \approx 0.22$, we deduce $R = 75\%$.

All subsequent data are taken through 30-μm-long slabs of photonic crystal, 15 unit cells thick. Measured transmission $T(u)$ (points) and their derivatives $\partial T(u)/\partial u$ (arrows) are reported for all samples in Fig. 2. Lines are guides to the eye. The four sets of data correspond to all four cases (TE, TM) $\times$ (ΓM, ΓK) of polarization and propagation direction.

For comparison, we show the theoretically predicted transmission of a triangular array of infinitely deep air cylinders in a uniform dielectric, below the experimental data. The theory is based on the transfer matrix method [19] which yields transmission, reflection, and in-plane diffraction coefficients. Parameters used in the calculation were $f = 28.5\%$, consistent with experimental values and dielectric constant $\varepsilon = 10.2$, somewhat lower than n_{eff} [6].

The general behavior of intensities as well as derivatives is very consistent with the calculation. In TE, the two overlapping stop bands at about $u = 0.25$, going down to the noise level, are particularly noteworthy and confirm previous measurements where only rising band edges (here between $u = 0.27$ and $u = 0.29$) were observed [6]. Clear falling band edges appear at $u = 0.2$ for ΓM and at $u = 0.23$ for ΓK. In the pass window between $u = 0.3$ and $u = 0.35$, transmission in excess of 50% is observed. The contrast between pass and stop windows exceeds three decades. In TM, a ΓM stop band inhibits transmission near $u = 0.21$, but does not overlap with the ΓK low-transmission window around $u = 0.26$,

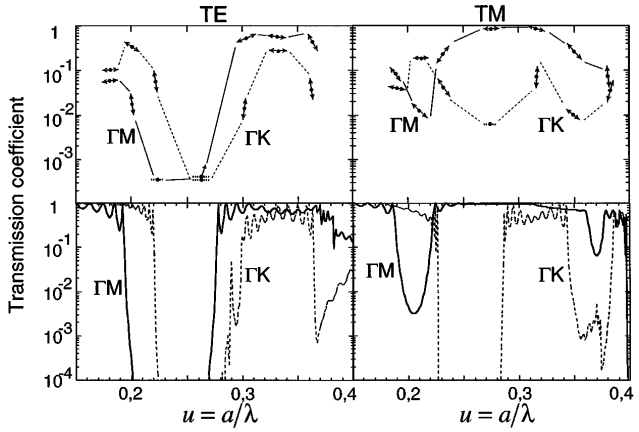

FIG. 2. Transmission data of PBG patterns for TE (left) and TM (right) polarizations. Dashed lines are for ΓK orientation, full lines are for ΓM orientation. Top frames: experiments. Each symbol is the mean value and the double arrow is the derivative. Small dotted lines represent the noise level. Lines are guides to the eye through the various samples. Bottom frames: theoretical predictions for a pure 2D PBG with air-filling factor $f = 28.5\%$ and matter dielectric constant $\varepsilon = 10.2$.

where transmission is at noise level. This does not correspond to a genuine stop band but results from a symmetry-forbidden coupling between the incident wave and the conduction band mode [6,20,21]. Note the impressive value of TM transmission along ΓM, over 80% for u between 0.25 and 0.3. It is the first time, to our knowledge, that such good agreement has been obtained over such a wide range of u values, both in terms of reduced energy dependence and absolute transmission values.

A crucial test that would ensure exclusive in-plane interaction is that low-transmission regimes coincide with high reflection. Figure 3 shows the reflection data obtained from fringe visibility. Unlike Fig. 2, we display data points, not derivatives, because there were not enough fringes in the 20 nm spectral window.

The four sets $(\mathrm{TE}, \mathrm{TM}) \times (\Gamma M, \Gamma K)$, compared to the theoretical curves of Fig. 3 (same parameters as above) again show a very satisfying agreement. The highest reflectivity of $R > 80\%$ was obtained for TE polarization propagating along ΓM, coinciding with the low-transmission window. TM reflectivities are significantly below theoretical predictions, but the relative position of the various curves and the overall spectral behavior is still maintained.

Reflection and transmission alone, however, do not tell the whole PBG story: Because of the periodic nature of PBG patterns, the in-plane interaction may also be largely diffractive. As discussed by Sakoda in [21], plane waves may be diffracted at angles predicted by the standard ruled grating formulas [18], using the surface period of the 30-μm-long PBG slab: a for ΓM and $\sqrt{3}\,a$ for ΓK. Conditions for diffraction at normal incidence are then $u \geq (n_{\mathrm{eff}})^{-1}$ for ΓM and $u \geq (\sqrt{3}\,n_{\mathrm{eff}})^{-1}$ for ΓK. Only below these cutoffs should one observe $R + T = 1$. Above, four beams are diffracted in first-Bragg orders at angle θ, two with efficiencies η_R and two with efficiencies η_T [Fig. 4(a)]. This is not a loss mechanism and does not preclude the use of PBG for spontaneous emission control: Lossless interaction with the structure now reads $R + T + D = 1$, where $D = 2\eta_R + 2\eta_T$ is the diffracted power for unit incident power.

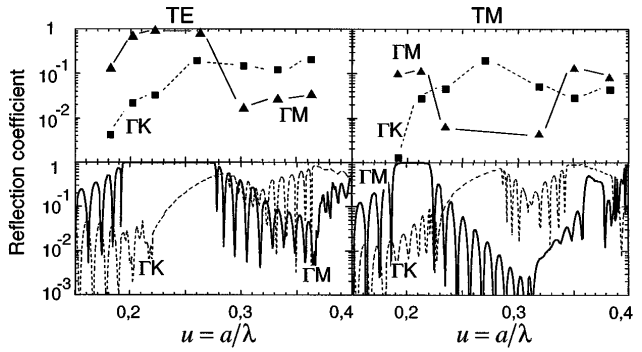

FIG. 3. Reflection data of PBG patterns for TE (left) and TM (right) polarizations. Dashed lines and square symbols are for ΓK orientation, full lines and triangular symbols are for ΓM. Top frames: experimental reflectivities deduced from fringe analysis. Lines are guides to the eye through the various samples. Bottom frames: theoretical predictions using the same parameters as for transmission.

Experimentally, the in-plane diffraction is detected in the geometry shown in Fig. 4. In transmission [Fig. 4(b)], guided light also appears at a point B, away from the direct beam in A. Recalling the $\sim 6^\circ$ directional selectivity achieved by our setup, light occurring at such a point can only have been redirected by the lattice from oblique incidence θ to normal incidence and is, therefore, an unambiguous signature of in-plane diffraction. The same holds for the reflection geometry of Fig. 4(c). The direct beam is seen at A', but light also emerges at B'. In both cases, one measures at B or B' the diffraction efficiency at oblique incidence θ if the reference is taken at a distance d''

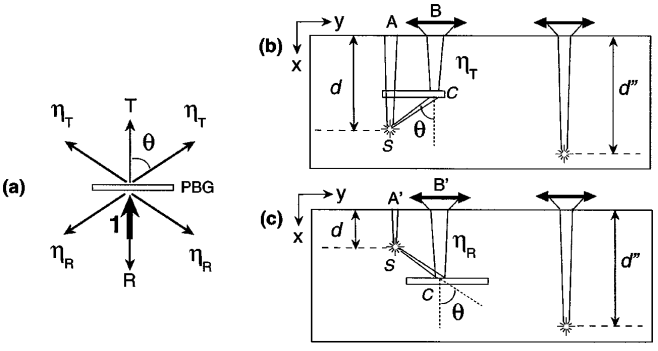

FIG. 4. (a) Definition of forward and backward diffraction efficiencies at angle θ with normal incidence. (b) In the experiment, light is forward diffracted along the x axis with oblique incidence θ. Redirected light exits the sample at point B, farther away from the direct beam in point A. Reference is taken with $d'' = SC + CB$. (c) Analogous configuration for backward diffraction.

from the edge, equal to the total diffracted light path ($d'' = SC + CB$ in Fig. 4). The result is, from calculation (and it can be shown by time reversal symmetry arguments), that a reciprocity rule holds for oblique to normal incidence and normal to oblique incidence diffraction efficiencies, so that the measured efficiencies in our experiment are the same η_R and η_T of Fig. 4(a).

As an example, let us consider the particular case $u = 0.22$ in TE. Data of Fig. 2 show transmission less than 10% along both ΓM and ΓK. While the reflection coefficient is over 80% along ΓM, it is very weak along ΓK (less than 5%). With $n_{\text{eff}} \approx 3.4$, the ΓM sample is below diffraction cutoff, while ΓK is above cutoff with a predicted diffraction efficiency $2\eta_R \approx 0.9$. We, indeed, measured $\eta_R \approx 40\%$ and $\eta_T \approx 0\%$, thus $D > \sim 80\%$. This result is again very consistent with theoretical predictions. Measurements on all samples allowed us to compare measured η_R and η_T with transfer matrix simulation, still using the same parameters as above. While η_R proved to be in good agreement with predictions, both quantitatively and for u values, η_T showed values lower than predictions, but with the same global behavior.

Finally, the consistency of the three coefficients R, T, and D with this theory shows that the 2D picture holds in the deep-etched guide configuration despite the lack of waveguiding in the holes and their finite height.

The quality of in-plane control achieved by each structure is estimated through the value of $\Sigma = R + T + D$. For all samples with period $a \geq 200$ nm ($u \geq 0.2$), we found $\Sigma > 70\%$ for TE polarization and propagation along ΓM, while samples with propagation along ΓK exhibit Σ values from 30% to 95%. The Σ values for TM polarization are generally lower, spanning from 12% to 90%. The $a = 180$ nm sample (u around 0.18) clearly showed Σ less than 20% in all four cases, which we attribute to shallower holes, due to etching limitations.

The detailed mechanisms responsible for these deviations from unity are not clear at the moment. The next step to clarify this issue should be the measurement of light scattered into the substrate and the air. However, in the optimal case of $a = 220$ nm ($u = 0.22$), Σ is more than 95% along both orientations for TE polarization, as well as for TM polarization along ΓK. Hence, we found a regime where the photonic crystal can be considered as a lossless dielectric that controls most of the emitted guided light, which is TE in our QWs. It is now important to understand whether the present limits are intrinsic or if more control can be gained by optimizing the waveguides and the PBG structures.

In summary, we have demonstrated that guided light can be reflected, transmitted, or diffracted by a 2D PBG pattern, depending on the wavelength to period ratio, i.e., on the photon energy compared to the photonic band gap frequency. This is the first evidence of such a degree of control of spontaneously emitted light in an integrated optics configuration. We have emphasized that very high diffraction coefficients can be obtained, which shows that PBGs in the gap should not be viewed as mere specular mirrors. Conversely, this efficient diffraction could be exploited for the realization of compact dispersive elements such as gratings in integrated optics systems using standard single-step lithographic techniques. In our view, these measurements validate, for the first time at such wavelengths, the hopes placed in photonic crystals, to efficiently "mold the flow of light" [3].

Part of this Letter is supported by the European Contract ESPRIT SMILES No. 8447. T. F. K. is supported by a Royal Society Research Fellowship and we thank the Nanoelectronics Research Centre at Glasgow University for technical support.

*Presently at California Institute of Technology, Mail stop 136-93, Pasadena, CA 91125.

†Permanent address: Groupe Photonique, Laboratoire d'Analyse et d'Architecture des Systémes-CNRS, 7, avenue du Colonel Roche, 31077 Toulouse Cedex, France.

[1] E. Yablonovitch, J. Mod. Opt. **41**, 173 (1994).
[2] *Photonic Bandgap Materials*, edited by C. M. Soukoulis (Kluwer, Dordrecht, 1996).
[3] J. D. Joannopoulos, R. D. Meade, and J. N. Winn, *Photonic Crystals, Molding the Flow of Light* (Princeton University Press, Princeton, NJ, 1995).
[4] A. Mekis *et al.*, Phys. Rev. Lett. **77**, 3787 (1996).
[5] C. C. Cheng *et al.*, J. Vac. Sci. Technol. B **14**, 4110 (1996).
[6] T. F. Krauss, R. M. De La Rue, and S. Brand, Nature (London) **383**, 699 (1996).
[7] H.-B. Lin, R. J. Tonucci, and A. J. Campillo, Appl. Phys. Lett. **68**, 2927 (1996).
[8] U. Grüning *et al.*, Appl. Phys. Lett. **68**, 747 (1996).
[9] T. Baba and T. Matsuzaki, in *Microcavities and Photonic Bandgaps: Physics and Applications*, edited by J. Rarity and C. Weisbuch (Kluwer, Dordrecht, 1996).
[10] S. Fan, P. R. Villeneuve, and J. D. Joannopoulos, Phys. Rev. Lett. **78**, 3294 (1997).
[11] P. L. Gourley *et al.*, Appl. Phys. Lett. **64**, 687 (1994).
[12] J. O'Brien *et al.*, Electron. Lett. **32**, 2243 (1996).
[13] P. St J. Russell, *et al.*, in *Microcavities and Photonic Bandgaps: Physics and Applications*, edited by J. Rarity and C. Weisbuch (Kluwer, Dordrecht, 1996), p. 203.
[14] P. Wittke, RCA Rev. **36**, 655 (1975).
[15] D. Labilloy *et al.*, Appl. Phys. Lett. **71**, 738 (1997).
[16] T. Krauss *et al.*, Electron. Lett. **30**, 1444 (1994).
[17] M. Plihal and A. A. Maradudin, Phys. Rev. B **44**, 8565 (1991).
[18] M. Born and E. Wolf, *Principles of Optics* (Pergamon Press, Oxford, 1980).
[19] J. B. Pendry and A. MacKinnon, Phys. Rev. Lett. **69**, 2772 (1992).
[20] W. M. Robertson *et al.*, Phys. Rev. Lett. **68**, 2023 (1992).
[21] K. Sakoda, Phys. Rev. B **52**, 8992 (1995).